Designing dielectric resonators on substrates: Combining magnetic and electric resonances

J. van de Groep* **and A. Polman**

Center for Nanophotonics, FOM Institute AMOLF, Science Park 104, 1098 XG, Amsterdam, Netherlands

*groep@amolf.nl

Abstract: High-performance integrated optics, solar cells, and sensors require nanoscale optical components at the surface of the device, in order to manipulate, redirect and concentrate light. High-index dielectric resonators provide the possibility to do this efficiently with low absorption losses. The resonances supported by dielectric resonators are both magnetic and electric in nature. Combined scattering from these two can be used for directional scattering. Most applications require strong coupling between the particles and the substrate in order to enhance the absorption in the substrate. However, the coupling with the substrate strongly influences the resonant behavior of the particles. Here, we systematically study the influence of particle geometry and dielectric environment on the resonant behavior of dielectric resonators in the visible to near-IR spectral range. We show the key role of retardation in the excitation of the magnetic dipole (MD) mode, as well as the limit where no MD mode is supported. Furthermore, we study the influence of particle diameter, shape and substrate index on the spectral position, width and overlap of the electric dipole (ED) and MD modes. Also, we show that the ED and MD mode can selectively be enhanced or suppressed using multi-layer substrates. And, by comparing dipole excitation and plane wave excitation, we study the influence of driving field on the scattering properties. Finally, we show that the directional radiation profiles of the ED and MD modes in resonators on a substrate are similar to those of point-dipoles close to a substrate. Altogether, this work is a guideline how to tune magnetic and electric resonances for specific applications.

OCIS codes: (140.4780) Optical resonators; (290.5850) Scattering, particles; (350.4238) Nanophotonics and photonic crystals.

References and links

1. J. A. Schuller, E. S. Barnard, W. Cai, Y. C. Jun, J. S. White, and M. L. Brongersma, "Plasmonics for extreme light concentration and manipulation," Nat. Mater. **9**, 193–204 (2010).
2. C. Höppener and L. Novotny, "Antenna-based optical imaging of single Ca^{2+} transmembrane proteins in liquids," Nano Lett. **8**, 642–646 (2008).
3. H. A. Atwater and A. Polman, "Plasmonics for improved photovoltaic devices," Nat. Mater. **9**, 205–213 (2010).
4. V. E. Ferry, M. A. Verschuuren, H. B. T. Li, E. Verhagen, R. H. Walters, R. E. I. Schropp, H. A. Atwater, and A. Polman, "Light trapping in ultrathin plasmonic solar cells," Opt. Express **18**, A237–A245 (2010).
5. M. K. Kwon, J. Y. Kim, B. H. Kim, I. K. Park, C. Y. Cho, C. C. Byeon, and S. J. Park, "Surface-plasmon-enhanced light-emitting diodes," Adv. Mater. **20**, 1253–1257 (2008).

#195676 - $15.00 USD Received 27 Aug 2013; revised 11 Oct 2013; accepted 16 Oct 2013; published 25 Oct 2013

6. N. Yu, R. Blanchard, J. Fan, Q. J. Wang, C. Pflügl, L. Diehl, T. Edamura, M. Yamanishi, H. Kan, and F. Capasso, "Quantum cascade lasers with integrated plasmonic antenna-array collimators," Opt. Express **16**, 19447–19461 (2008).
7. C. F. Bohren and D. R. Huffman, *Absorption and Scattering of Light by Small Particles* (Wiley, 2008).
8. C. M. Soukoulis and M. Wegener, "Past achievements and future challenges in the development of three-dimensional photonic metamaterials," Nat. Photonics **5**, 523–530 (2011).
9. Q. Zhao, J. Zhou, F. Zhang, and D. Lippens, "Mie resonance-based dielectric metamaterials," Mater. Today **12**, 60–69 (2009).
10. L. Huang, Y. Yu, and L. Cao, "General modal properties of optical resonances in subwavelength nonspherical dielectric structures," Nano Lett. **13**, 3559–3565 (2013).
11. Y. H. Fu, A. I. Kuznetsov, A. E. Miroschnichenko, Y. F. Yu, and B. Luk'yanchuk, "Directional visible light scattering by silicon nanoparticles," Nat. Commun. **4**, 1527 (2013).
12. G. Mie, "Beitrge zur optik trber medien, speziell kolloidaler metallsungen," Ann. Phys. **330**, 377–445 (1908).
13. A. García-Etxarri, R. Gómez-Medina, L. S. Froufe-Pérez, C. López, L. Chantada, F. Scheffold, J. Aizpurua, M. Nieto-Vesperinas, and J. J. Sáenz, "Strong magnetic response of submicron silicon particles in the infrared," Opt. Express **19**, 4815–4826 (2011).
14. A. B. Evlyukhin, C. Reinhardt, A. Seidel, B. S. Luk'yanchuck, and B. N. Chichkov, "Optical response features of Si-nanoparticle arrays," Phys. Rev. B **82**, 045404 (2010).
15. J. A. Schuller and M. L. Brongersma, "General properties of dielectric optical antennas," Opt. Express **17**, 24084–24095 (2009).
16. A. I. Kuznetsov, A. E. Miroschnichenko, Y. H. Fu, J. B. Zhang, and B. Luk'yanchuk, "Magnetic light," Sci. Rep. **2**, 492 (2012).
17. A. B. Evlyukhin, C. Reinhardt, and B. N. Chichkov, "Multipole light scattering by nonspherical nanoparticles in the discrete dipole approximation," Phys. Rev. B **84**, 235429 (2011).
18. A. B. Evlyukhin, S. M. Novikov, U. Zywietz, R. L. Eriksen, C. Reinhardt, S. I. Bozhevolnyi, and B. N. Chichkov, "Demonstration of magnetic dipole resonances of dielectric nanospheres in the visible region," Nano Lett. **12**, 3749–3755 (2012).
19. M. K. Schmidt, R. Esteban, J. J. Sáenz, I. Suárez-Lacelle, S. Mackowski, and J. Aizpurua, "Dielectric antennas - a suitable platform for controlling magnetic dipolar emission," Opt. Express **20**, 13636–13650 (2012).
20. S. Person, M. Jain, Z. Lapin, J. J. Sáenz, G. Wicks, and L. Novotny, "Demonstration of zero optical backscattering from single nanoparticles," Nano Lett. **13**, 1806–1809 (2013).
21. I. Staude, A. E. Miroshnichenko, M. Decker, N. T. Fofang, S. Liu, E. Gonzales, J. Dominguez, T. S. Luk, D. N. Neshev, I. Brener, and Y. Kivshar, "Tailoring directional scattering through magnetic and electric resonances in subwavelength silicon nanodisks," ACS Nano **7**, 7824–7832 (2013).
22. P. Fan, K. C. Y. Huang, L. Cao, and M. L. Brongersma, "Redesigning photodetector electrodes as an optical antenna," Nano Lett. **13**, 392–396 (2013).
23. P. Spinelli, M. A. Verschuuren, and A. Polman, "Broadband omnidirectional antireflection coating based on subwavelength surface Mie resonators," Nat. Commun. **3**, 692 (2012).
24. P. Spinelli, B. Macco, M. A. Verschuuren, W. M. M. Kessels, and A. Polman, "Al2O3/TiO2 nano-pattern antireflection coating with ultralow surface recombination," Appl. Phys. Lett. **102**, 233902 (2013).
25. FDTD Solutions, Lumerical Solutions, Inc., http://www.lumerical.com.
26. E. D. Palik, *Handbook of Optical Constants of Solids* (Academic, 1985).
27. P. Spinelli, C. van Lare, E. Verhagen, and A. Polman, "Controlling Fano lineshapes in plasmon-mediated light coupling into a substrate," Opt. Express **19**, A303–A311 (2011).
28. T. Coenen, J. van de Groep, and A. Polman, "Resonant Mie modes of single silicon nanocavities excited by electron irradiation," ACS Nano **7**, 1689–1698 (2013).
29. F. J. García de Abajo, "Optical excitations in electron microscopy," Rev. Mod. Phys. **82**, 209–275 (2010).
30. R. Sapienza, T. Coenen, J. Renger, M. Kuttge, N. F. van Hulst, and A. Polman, "Deep-subwavelength imaging of the modal dispersion of light," Nat. Mater. **11**, 781–787 (2012).
31. T. Coenen, E. J. R. Vesseur, and A. Polman, "Deep subwavelength spatial characterization of angular emission from single-crystal Au plasmonic ridge nanoantennas," ACS Nano **6**, 1742–1750 (2012).
32. K. G. Lee, X. W. Chen, H. Eghlidi, P. Kukura, R. Lettow, A. Renn, V. Sandoghdar, and S. Gotzinger, "A planar dielectric antenna for directional single-photon emission and near-unity collection efficiency," Nat. Photonics **5**, 166–169 (2011).
33. W. Lukosz and R. E. Kunz, "Light emission by magnetic and electric dipoles close to a plane interface. I. Total radiated power," J. Opt. Soc. Am. **67**, 1607–1614 (1977).
34. L. Novotny and B. Hecht, *Principles of Nano-Optics* (Cambridge University, 2006).
35. M. Kerker, D. Wang, and G. Giles, "Electromagnetic scattering by magnetic spheres," J. Opt. Soc. Am. **73**, 765–767 (1983).

#195676 - $15.00 USD Received 27 Aug 2013; revised 11 Oct 2013; accepted 16 Oct 2013; published 25 Oct 2013

1. Introduction

High-performance integrated optics, solar cells, sensors and many other optical devices require the ability to concentrate, redirect and manipulate light at the surface of the device, in order to optimize the coupling and trapping of light. Resonant nanostructures can have large scattering cross sections at visible wavelengths, and therefore are suitable candidates for this purpose. Plasmonic nanostructures have proven to be very successful in this field, and have been used for light focusing and scattering in sensing and imaging [1, 2], solar cells [3, 4] and light emitting devices [5, 6]. However, the performance of plasmonic nanostructures is always limited by parasitic absorption in the metal. High-index dielectric or semiconductor nanostructures support (Mie-like) geometrical resonances in the visible spectral range [7–10]. Unlike in plasmonic particles, these are driven by displacement currents rather than actual currents [11]. Therefore, these resonances are characterized by (very) low losses. Scattering from spherical dielectric particles in a homogeneous medium has already been described in great detail using Mie theory [12–15], and particles weakly coupled to the substrate have also been analyzed [16]. This work has shown that silicon nanoparticles support both electrical and magnetic resonances in the visible and near-infrared spectral range [13, 14, 16–19]. Recently, it has also been shown that the interplay between electrical and magnetic resonances can be used to control the angular radiation pattern of the resonant cavities [11, 20, 21], and that using cylinders instead of spheres allows for tuning of the spectral spacing between the electric and magnetic lowest order resonances [17, 21]. For all practical applications particles are placed on a substrate and in most cases strong coupling to the substrate is even desired (e.g. absorption in photodiodes [22], solar cells [23, 24], etc.). This interaction with the substrate strongly influences the resonant behavior, as well as the interaction between the magnetic and electric resonances. So far, there has been no systematic study on the influence of particle geometry and dielectric environment on the resonant properties of dielectric nanoparticles on a substrate.

Here, we use numerical simulations to systematically study the resonant properties of high-index dielectric particles in the visible spectral range for different particle geometries and dielectric environments. We show how electric and magnetic resonances are supported, and that retardation plays a key role in the driving of the magnetic resonances. Also, we show how varying the height and diameter of resonant nanocylinders placed on a dielectric substrate provides the possibility to spectrally tune the electric dipole (ED) and magnetic dipole (MD) resonances. Furthermore, we study how the presence of a (high-index) substrate dramatically alters the resonant properties, as well as the interplay between the different eigenmodes. We show that by tuning the substrate geometry, the ED and MD resonances can be selectively enhanced or suppressed. Also, we find that such resonators can be used as low-loss antennas that exhibit directional emission into the substrate. Altogether, this work shows how, by engineering the particle shape and dielectric environment, the scattering properties of single resonators placed on a dielectric substrate can be tailored for specific applications.

2. Magnetic and electric modes in dielectric particles

The ability to excite magnetic (dipolar) resonances in silicon particles, as well as the driving mechanism, has been described recently [13, 16, 18]. In short, the in-plane magnetic dipole is driven by the electric field of light that couples to displacement current loops, vertically oriented in the particle (see inset in Fig. 1(a)). This displacement current loop (orange) induces a magnetic dipole moment (blue), oriented perpendicular to the electric field polarization. Efficient driving of this displacement current loop requires significant retardation of the driving field (red) throughout the particle, as the electric field should undergo a significant phase shift in order to match the opposing electric field orientation in the top and bottom part of

#195676 - $15.00 USD Received 27 Aug 2013; revised 11 Oct 2013; accepted 16 Oct 2013; published 25 Oct 2013

the particle. The excitation of electric (dipolar) resonances on the other hand, only requires collective polarization of the material inside the resonator by the electric field component of the incident light.

Here, we systematically study the nature of the resonances supported by (mostly cylindrical) nanoparticles while changing the particle height, diameter, shape, presence and refractive index of a substrate, thickness of multi-layered substrates and driving field. To this end, we use finite-difference time-domain simulations [25] to calculate the normalized scattering cross section (scattering cross section normalized to geometrical cross section) $Q_{scat} = \sigma_{scat}/\sigma_{geo}$ and modal field profiles inside the particles. A total-field scattered-field source (TFSF) source is used, which launches a broad-band ($\lambda = 400 - 1000$ nm) plane wave from the top under normal incidence and filters out all the light that has not been scattered. Power transmission monitors are positioned around the TFSF source to monitor the power of the scattered field, and field monitors are positioned in and around the particle to monitor the local field intensity. Substrates (when used) have a purely real refractive index n_{sub}, to prevent absorption of the scattered light before reaching the power monitors. Perfectly Matching Layers (PMLs) are used to prevent any unphysical scattering from the simulation boundaries, and to mimic semi-infinite substrates. Optical constants for Si and SiO_2 are taken from Palik [26]. Automatic non-uniform meshes are used, and a 2.5 nm refinement mesh around the particle when monitoring the near-field intensities. Identification of the modes (MD, ED) is done by studying the field profiles inside the particle and identifying the corresponding current loops.

3. Retardation and particle height

We start by investigating the role of particle height on the excitation of resonant modes in crystalline Si cylinders in a homogeneous air environment. We choose Si since this is a high-index material with relatively low absorption losses in the visible and near-IR, and has been used in most previous work on magnetic resonances [11, 13, 16, 18, 21, 23]. The necessity of field retardation for the excitation of the MD mode suggests that if the particle is shallow enough, there should not be enough retardation to drive a displacement current loop, and therefore a MD resonance cannot be supported. The ED mode however, does not need retardation *inside* the particle: since $\mu = 1$ both inside and outside the particle, the magnetic current loop induced by the dipole moment can also extend outside the particle.

To study the effect of particle height on retardation, we calculate Q_{scat} for a Si cylinder in air, with diameter $d = 100$ nm and height $h = 100$ nm. Figure 1(a) shows Q_{scat} as a function of wavelength. Two clear peaks are observed which correspond to the ED mode at $\lambda = 440$ nm and the MD mode at $\lambda = 503$ nm. As mentioned above, identification of the modes (MD, ED) is done by studying the field profiles inside the particle and identifying the corresponding current loops. Figure 1(b) shows Q_{scat} spectra for particle heights in the range $h = 50 - 250$ nm. The vertical dashed line represents the crosscut shown in Fig. 1(a). The two maxima, labeled ED and MD, show a clear red-shift and increase in Q_{scat} for increasing h. Note that two peaks can be observed for the entire range of h, even down to 50 nm. Thus, even a cylinder only 50 nm high supports a vertically-oriented displacement current loop generating a MD resonance. The strong increase in Q_{scat} for larger height is due to the fact that the volume of the particle increases and thus the polarizability and thereby σ_{scat}, while the geometrical cross section σ_{geo} does not change. Unlike plasmonic particles, where an increase in h gives rise to a small blue-shift for an in-plane dipole mode due to an increased restoring force, higher Si cylinders give rise to a large red-shift that saturates above $h \sim 220$ nm. This can be understood from Figs. 1(c)–1(e), which show vertical crosscuts parallel to the polarization of the driving

#195676 - $15.00 USD Received 27 Aug 2013; revised 11 Oct 2013; accepted 16 Oct 2013; published 25 Oct 2013

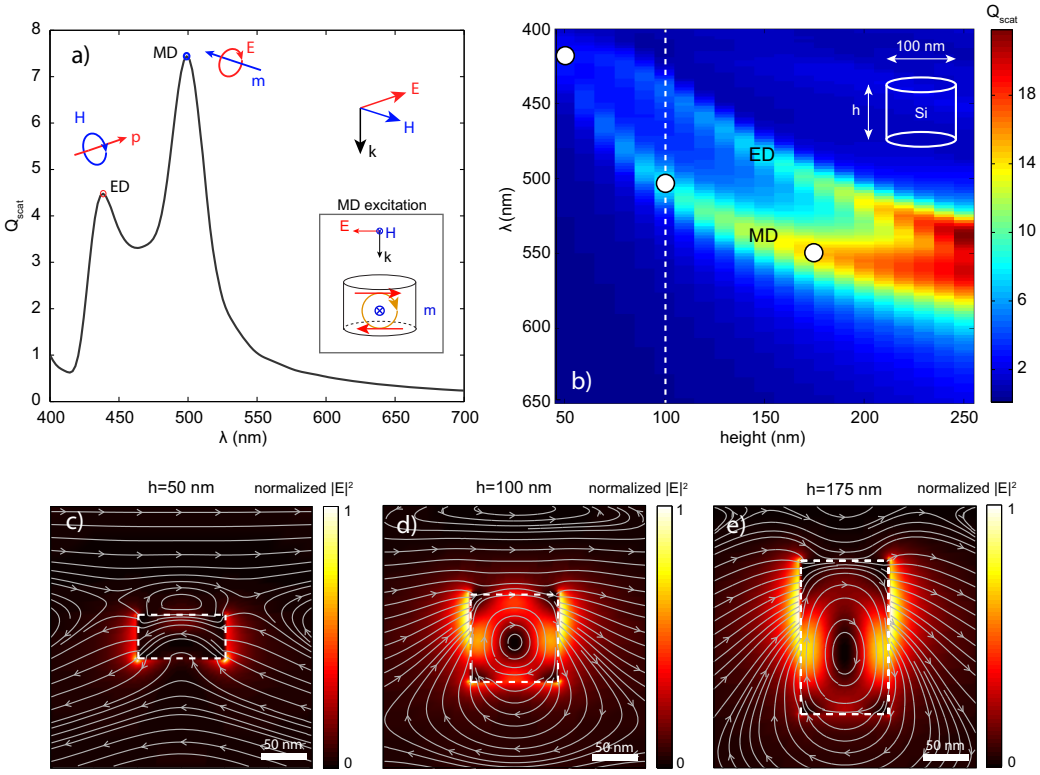

Fig. 1. **(a)** Q_{scat} as a function of wavelength for a Si cylinder in air with $h = 100$ nm and $d = 100$ nm for optical excitation under normal incidence. The peaks correspond to the ED and MD mode, and the corresponding dipole moments and current loops are shown. The polarization of the driving field is shown in the top right. The inset shows the excitation mechanism of the MD mode. **(b)** Q_{scat} (color) as a function of λ and h for $h = 50 - 250$ nm. The particle geometry is shown as an inset. The vertical white line is the crosscut corresponding to the spectrum shown in (a). The white dots correspond to the λ - h combinations used for (c-e). **(c-e)** Normalized electric field intensity $|E|^2$ (color) and electric field lines (gray) in vertical crosscuts through particles with $h = 50$ nm (c), $h = 100$ nm (d) and $h = 175$ nm (e), parallel to the electric driving field.

field of the normalized electric field intensity distribution $|E|^2$ (color) for $h = 50$ nm (c), $h = 100$ nm (d) and $h = 175$ nm (e). Electric field lines (gray) in this plane at resonance are also plotted. The three combinations of h and λ from Figs. 1(c)–1(e) are indicated by white dots in Fig. 1(b). In Figs. 1(d) and 1(e), both the intensity profiles and the field lines clearly show the loop induced by the driving field, which in turn drives the out-of-plane MD mode. In (c) however, this loop is not clearly visible. Detailed analysis of crosscuts through other planes (not shown here) do show that there is a current loop. But, a large fraction of the current loop is inside the evanescent near field in the air below the particle, where $n = 1$ (hence the high field intensity at the bottom corners). As the particle gets taller, Figs. 1(d) and 1(e), the current loop fits better inside the particle and a larger fraction of the field is in the high index medium, giving rise to a red-shift which saturates when the current loop easily fits inside. A similar argument holds for the ED mode, where a larger fraction of the field is inside the cylinder for larger h, giving rise to a red-shift.

#195676 - $15.00 USD Received 27 Aug 2013; revised 11 Oct 2013; accepted 16 Oct 2013; published 25 Oct 2013

Concomitant with the strong blue-shift for smaller h, the index of Si also strongly increases for smaller wavelengths (from $n = 4$ at $\lambda = 550$ nm to $n = 5.1$ at $\lambda = 420$ nm). This makes the particles "optically" higher, thus creating more space for a current loop and as a result, the MD mode does not disappear. Note that for a non-dispersive medium this might not be the case.

Figure 2(a) shows Q_{scat} as a function of wavelength for a $d = 250$ nm cylinder in air, made of a non-dispersive dielectric with $n = 2$ for different heights in the range $h = 50 - 200$ nm. For $h = 50 - 100$ nm, one very broad peak is observed, which corresponds to the ED mode. When $h > 100$ nm, there is enough retardation to support a displacement current loop and the MD resonance is supported as well, which then red-shifts for larger h, as explained above. Note that the Q-factor of the resonances is much lower than observed in Fig. 1(a) since the lower index of the particle results in poor mode confinement and thus a large radiative loss rates γ_{rad}. Therefore, the ED and the MD spectrally overlap and one broad ED/MD peak is observed. Also note that the identification of the modes is again done by studying the field profiles. In this case however, the ED and MD modes spectrally overlap, such that in the near-field profiles both dipolar field profiles and corresponding current loops can be distinguished. The relatively sharp peak that appears in the blue spectral range for larger heights corresponds to the magnetic quadrupole mode (MQ), as will be shown later. Thus, in the limit that there is not enough retardation of the driving field inside the particle (low n and h), the MD mode is not supported, whereas the ED mode is always supported.

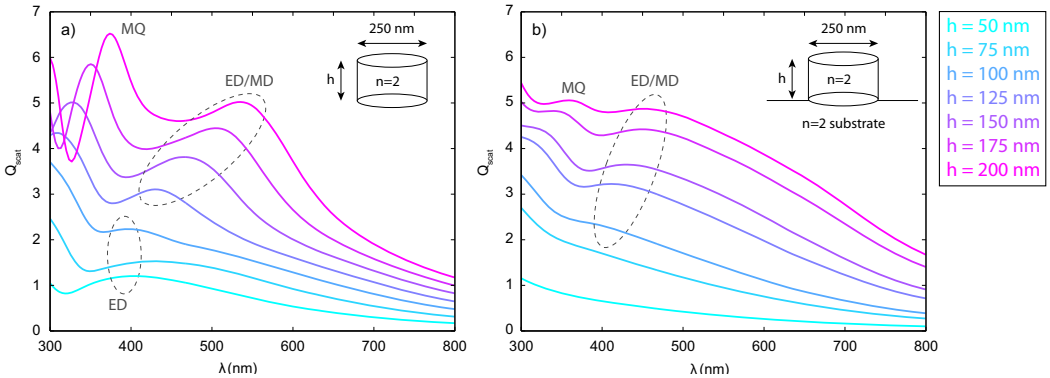

Fig. 2. **(a)** Q_{scat} as function of wavelength for $d = 250$ nm particles made of a non-dispersive dielectric with $n = 2$, plotted for heights in the range $h = 50 - 200$ nm. The geometry is shown as an inset. The peaks are labeled according to the resonance they correspond to (MD, ED, MQ). For $h < 125$ nm, no MD is supported. **(b)** Q_{scat} for the same particles as in (a), but now on a semi-infinite substrate wih $n = 2$ (see inset for geometry).

It has been shown that when a dielectric resonator is positioned on a substrate with similar index as the resonator, the displacement current loop can extend into the substrate [23] (also see section 5). The substrate effectively provides additional "optical" height to the resonator, such that the MD mode can be supported for shallow particles that do not show this resonance when positioned in air. Figure 2(b) shows Q_{scat} for the same resonator as in (a), but now positioned on a semi-infinite substrate with $n_{sub} = 2$ (see inset). Comparison of (a) and (b) clearly shows that all resonances have significantly broadened, due to the fact that part of the mode profile extends into the substrate. This increases the radiative loss rate γ_{rad} into the substrate,

#195676 - $15.00 USD Received 27 Aug 2013; revised 11 Oct 2013; accepted 16 Oct 2013; published 25 Oct 2013

resulting in a reduced resonance Q-factor. Although combining shallow particles ($h < 100$ nm) with a substrate provides enough retardation and space to support a current loop, the degree of confinement is insufficient to support any resonance. However, as soon as resonant behavior occurs by increasing h, the resonant peak corresponds to a combination of the ED and MD eigenmodes.

4. Particle diameter and higher order modes

Increasing the particle diameter d enables the excitation of resonant modes at larger wavelengths. A rule of thumb for the resonant wavelengths of the dipolar modes of resonant nanocylinders in air is $\lambda/n \sim d$. Furthermore, when the diameter is large enough, higher-order modes will also be supported in the visible spectral range. In Fig. 3 we investigate the spectral spacing of the ED and MD modes. Figure 3(a) shows Q_{scat} (color) for $h = 100$ nm Si cylinders in air, with varying diameter in the range $d = 50 - 250$ nm.

For $d < 130$ nm two clear resonances are present, which correspond to the ED and MD modes, as was observed in Fig. 1 where the particle height was varied. As d increases, both modes strongly red-shift and start to overlap spectrally as $d > 160$ nm, while the peak value of Q_{scat} stays roughly constant (~ 8). The curvature of the MD branch is a result of the dispersive nature of the Si. Note that the red-shift for the ED mode with increasing d is much stronger than that of the MD mode, such that tuning the particle aspect ratio allows for control over the spectral spacing between the ED and MD mode. In fact, a further increase in diameter will cause the ED and MD branch in Fig. 3(a) to cross as shown in [21]. The vertical crosscut in Fig. 3(a) indicated by the white line at $d = 175$ nm, is shown as the red spectrum in Fig. 3(c). The spectrum shows how the ED mode appears as a shoulder on the dominant MD resonance. Thus, in air, the ED and MD peaks are spectrally separated for small d and spectrally overlapping for large d. A third peak is observed for around $\lambda = 466$ nm, which also red-shifts with increasing d. This peak is due to a magnetic quadrupole (MQ) as appears from Fig. 3(d), which shows a vertical crosscut, parallel to the H-field of the driving field, of the normalized magnetic field intensity $|H|^2$ (color) and the magnetic field lines (gray lines) in a $d = 175$ nm particle at the MQ resonance wavelength ($\lambda = 466$ nm). The combination of d and λ used for this plot is indicated with a white dot in Fig. 3(a). The crosscut shows four bright lobes in the corners of the particle (the bottom two overlap, giving a bright spot in the center), corresponding to the four poles of a quadrupole. The field lines show which pole is positive (field lines going out of the particle) and negative (field lines going in), indicated by white $+$ and $-$ signs. The observed mode sequence MD-ED-MQ with decreasing resonance wavelengths in Figs. 3(a) and 3(c) is in agreement with the well established mode hierarchy of magnetic and electric modes in spheres [12, 16]. Note that a strong reduction in the cylinder aspect ratio can cause the MD mode to be positioned at lower wavelength than the ED mode, thereby changing this mode hierarchy [21].

Figure 3(b) shows Q_{scat} for the same resonators as in (a), but now on a semi-infinite substrate with $n_{sub} = 3.5$ (roughly equal to n_{Si}, see inset for geometry). Comparing (a) and (b), four characteristic differences are observed. First, the ED and MD modes in (b) are spectrally broader and overlapping, now also for small d, which is a result of the increase of γ_{rad} into the substrate. Second, the peak values for Q_{scat} are much higher for small d (~ 11 instead of ~ 8) and for the MQ mode (~ 7 instead of ~ 5). Both the first effect (broadening) and second effect (increase in Q_{scat}) are attributed to the increased local density of optical states (*LDOS*) accessible to the resonator when located on a substrate: there are more radiative states available to couple to, thus increasing γ_{rad} and therefore Q_{scat}. Third, for $d > 160$ nm the ED/MD peak becomes

#195676 - $15.00 USD Received 27 Aug 2013; revised 11 Oct 2013; accepted 16 Oct 2013; published 25 Oct 2013

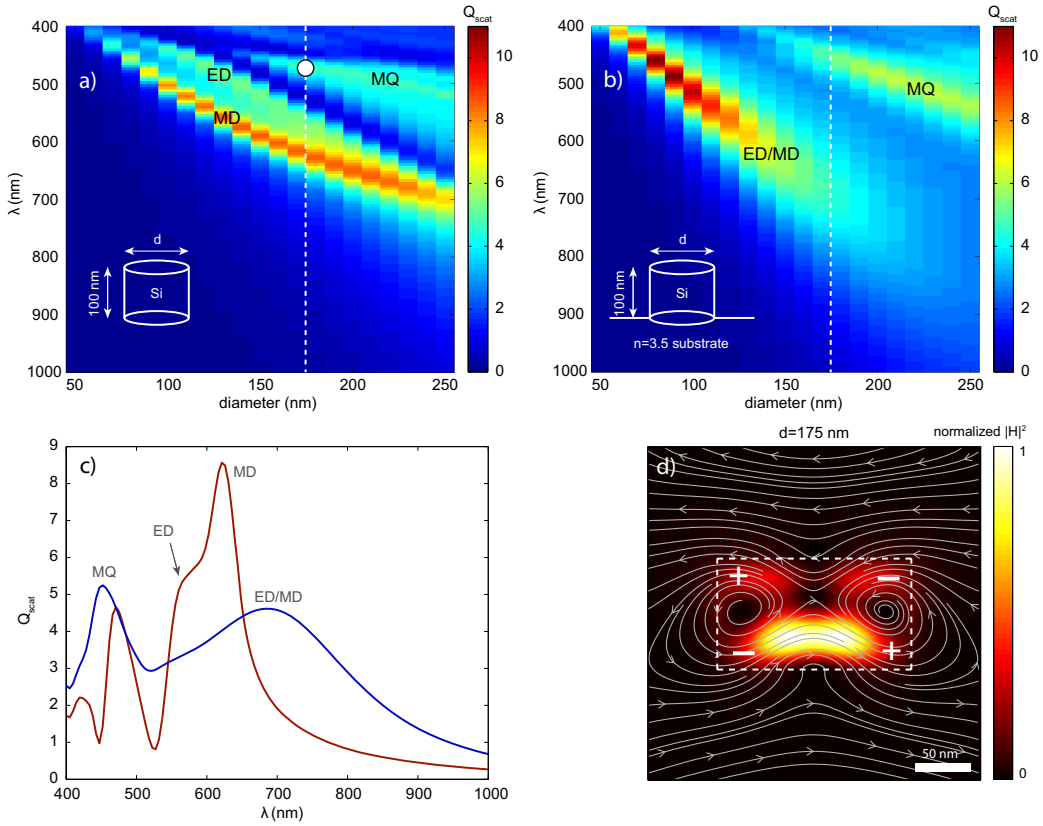

Fig. 3. **(a)** Q_{scat} (color) as a function of wavelength for a $h = 100$ nm Si cylinder in air, for diameters in the range $d = 50 - 250$ nm. The geometry is shown as an inset. The peaks are labeled according to the resonance they correspond to (ED,MD,MQ). **(b)** Q_{scat} (color) for the same resonator as in (a), but now on a semi-infinite substrate with $n = 3.5$ (see inset). **(c)** Spectra corresponding to crosscuts indicated by white certical dashed lines in (a) and (b) showing the spectra for $d = 175$ nm, in air (red) and on a $n = 3.5$ substrate (blue). The labels indicate the corresponding resonant modes. **(d)** Vertical crosscut through the resonator in air ($d = 175$ nm, see white dot in (a)) in the plane parallel to the H-field of the driving field for $\lambda = 466$ nm. Plotted is the normalized $|H|^2$ (color) and the magnetic field lines (gray), showing the MQ mode profile. The corresponding poles are labeled with $+$ and $-$ signs (white).

very broad, scattering light over the entire visible spectral range, since a larger fraction of the mode profile extends into the substrate for larger λ. Figure 3(c) (blue) shows the spectrum for $d = 175$ nm. Clearly, the ED/MD peak ranges all the way from $\lambda = 400$ nm up to $\lambda = 1000$ nm. These modes can serve to achieve efficient light coupling into a high-index substrate over a broad spectral range, as shown in [23, 24]. Fourth, the red-shift of the ED/MD peak is more dramatic than in (a), which is a result of the fact that a large fraction of the near-field of the resonance is inside the $n = 3.5$ substrate instead of air ($n = 1$).

#195676 - $15.00 USD Received 27 Aug 2013; revised 11 Oct 2013; accepted 16 Oct 2013; published 25 Oct 2013

5. Substrate index and particle shape

Sections 3 and 4 have shown that when a cylindrical resonator is positioned on a substrate with $n_{sub} \sim n_{part}$, the ED and MD resonances broaden and spectrally overlap. Next, we investigate the case of $1 < n_{sub} < n_{part}$. We study how the spectral positions of the resonances depend on substrate index and particle shape. Figure 4(a) shows Q_{scat} for the same resonator as in Fig. 1(a), a Si cylinder with $d = 100$ nm and $h = 100$ nm, but now on a semi-infinite substrate with an index in the range $1 \leq n_{sub} \leq 3.5$, varying in steps of 0.25.

Figure 4(a) shows three characteristic features. First, as was observed in Figs. 2(b) and 3(b), increasing n_{sub} from 1 to 3.5 gradually broadens the resonance peaks (due to an increase in γ_{rad}) and causes the ED and MD peaks to overlap spectrally, such that the ED mode becomes a shoulder of the MD mode for high index. For $n_{sub} > 2.25$, the ED is no longer visible as a separate peak. Second, a significant increase in Q_{scat} is observed for increasing n_{sub}, which is attributed to the increase in the *LDOS* at the position of the particle. Third, a small red-shift is observed with increasing n_{sub}: $\lambda_{MD} = 499$ nm for $n_{sub} = 1$ and $\lambda_{MD} = 515$ nm for $n_{sub} = 3.5$. This is caused by the index experienced by the near-field of the resonance. Note that this small shift of only 16 nm is in sharp contrast with the dramatic 600 nm red-shift observed for a plasmonic dipolar resonance of a similar cylinder made of Ag [27]. This contrast is a direct result of the different nature of the resonance. While in plasmon resonances most light is concentrated at the interface (in direct contact with the substrate), in case of dielectric resonators most light is concentrated inside the resonator, making it less sensitive to substrate index.

To investigate the influence of particle shape, Fig. 4(b) shows Q_{scat} as a function of wavelength for the same cylinder as in (a) (red), a $d = 114$ nm sphere (green), and a cube with sides of length $l = 92$ nm (blue). The particles have the same volume, are all made of Si and the geometries are shown below (a) and (b). The dashed lines in Fig. 4(b) correspond to particles in air, the solid line to particles on a semi-infinite substrate with $n_{sub} = 3.5$. Note that the sphere is sticking 7 nm into the substrate (center is at 50 nm height above the substrate) to prevent unphysical hot spots at the infinitely sharp contact area (see sketched geometry). Figure 4(b) shows that both in air and on a substrate, the shape of the particle has only a small influence on the resonance wavelengths of the ED and MD modes. Both resonances are supported for all shapes, and the cylinder proves to be the most efficient scatterer. Furthermore, for all shapes Q_{scat} increases significantly due to the enhanced *LDOS*, when put onto a substrate. However, comparing the solid lines with the dashed lines shows that both the cylinder (red) and the cube (blue) show the dramatic broadening of the ED and MD resonances when compared to the case in air, causing the ED to appear as a shoulder on top of the MD mode. For the sphere (green), the broadening is significantly less and the ED remains to be a separate peak.

To understand this difference, we plot vertical crosscuts (parallel to the E-field of the driving field) through the center of all particles on the $n_{sub} = 3.5$ semi-infinite substrate, at the MD resonance wavelength. Figures 4(c)–4(e) show the normalized $|E|^2$ (color) and the electric field lines (gray), while Figs. 4(f)–4(h) show the normalized $|H|^2$ (color). The magnetic field lines are not plotted because $H \sim 0$ in this plane, which is perpendicular to the H-field orientation of the driving field. Figures 4(c)–4(e) clearly show the displacement current loops that induce the magnetic dipole $\vec{m}$ of the MD mode. Both (c) and (e) show that for the cylinder and the cube a significant fraction of the displacement current loop extends into the substrate. For the sphere, despite the fact that it sticks into the substrate, this effect is much smaller.

#195676 - $15.00 USD Received 27 Aug 2013; revised 11 Oct 2013; accepted 16 Oct 2013; published 25 Oct 2013

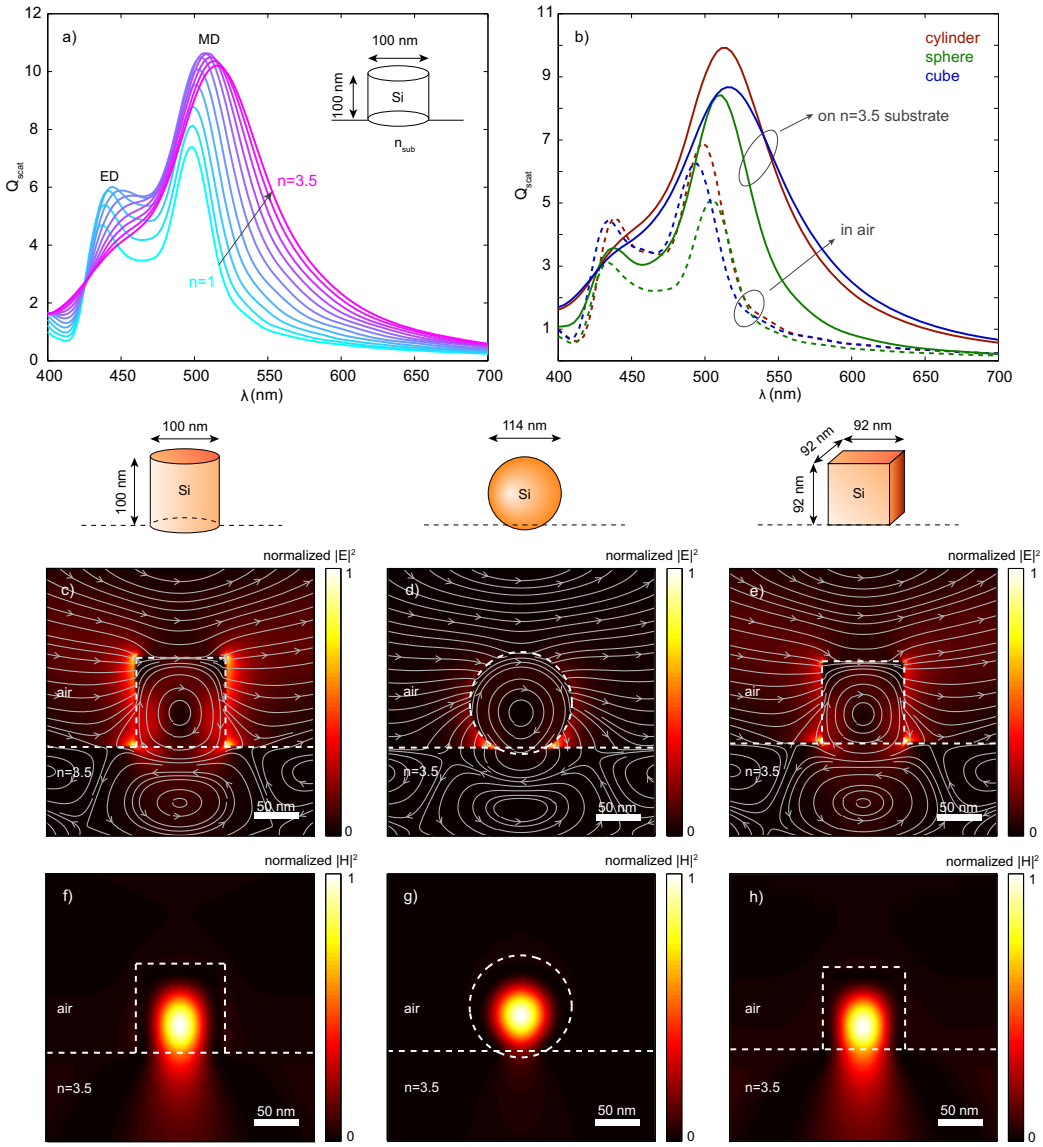

Fig. 4. **(a)** Q_{scat} as a function of wavelength for a Si cylinder with $h = 100$ nm, $d = 100$ nm, on a semi-infinite substrate with $1 \leq n_{sub} \leq 3.5$, in index steps of 0.25. The geometry is shown as an inset. **(b)** Q_{scat} for the same cylinder (red), a $d = 114$ nm sphere (green), and a $l = 92$ nm cube (blue) in air (dashed), all on a $n_{sub} = 3.5$ semi-infinite substrate (solid). All particles consist of Si and have the same volume. The three geometries are sketched below (a) and (b). Note that the sphere sticks 7 nm into the substrate to prevent an infinitely sharp contact area. **(c-e)** Vertical crosscuts through the center of all three particles in the plane parallel to the E-field of the source, showing the normalized $|E|^2$ (color) and electric field lines (gray). The particle surroundings and air-substrate interface are indicated with white dashed lines. The respective geometries are shown above the figures. The displacement current loops are clearly visible. **(f-h)** The same crosscuts as in (c-e), now showing the normalized $|H|^2$ (color) of the MD modes. The magnetic field lines are not plotted since $H \sim 0$ in this plane (perpendicular to source $\vec{H}$)

#195676 - $15.00 USD Received 27 Aug 2013; revised 11 Oct 2013; accepted 16 Oct 2013; published 25 Oct 2013

As a result, the coupling to the substrate is much weaker for the sphere than for the cylinder and cube. This is also clearly observable in Figs. 4(f)–4(h), which show that the magnetic field profile of the MD mode inside the substrate is much brighter for the cylinder and the cube, when compared to the sphere. The contact area of the resonator with the substrate is thus very important to get strong coupling to the substrate and provides tunability of the radiation rate γ_{rad} into the substrate. Note that in Figs. 4(c)–4(e) a second (reversed) current loop can be observed in the substrate below the particles. We attribute this to image dipoles induced by the dipole moments in the particles.

6. Selective mode enhancement with multi-layer substrates

Based on the results from sections 3-5 it is possible to design any resonator geometry such that the particle is resonant at the desired wavelength. Furthermore, by tuning the diameter and height separately it is possible to either have two spectrally separated ED/MD resonances (using a small diameter, large height) or spectrally overlapping resonances (large diameter, small height). However, for specific applications it may be useful to selectively select one of the two modes to dominate the response of the resonator; the ED or the MD mode.

This may be particularly relevant if the radiation pattern of the resonator is important, such as for example in light trapping geometries in photodiodes and solar cells, as will be shown in section 8. Here we will show that this can be done using a multi-layer substrate. The inset of Fig. 5(a) shows the proposed geometry: a Si cylinder with $d = 100$ nm and $h = 100$ nm is positioned on a SiO_2 layer with thickness t, which is on top of a $n_{sub} = 3.5$ substrate (e.g. Si). We vary the SiO_2 layer thickness from $0 \leq t \leq 500$ nm in steps of 20 nm and for each t we calculate Q_{scat}.

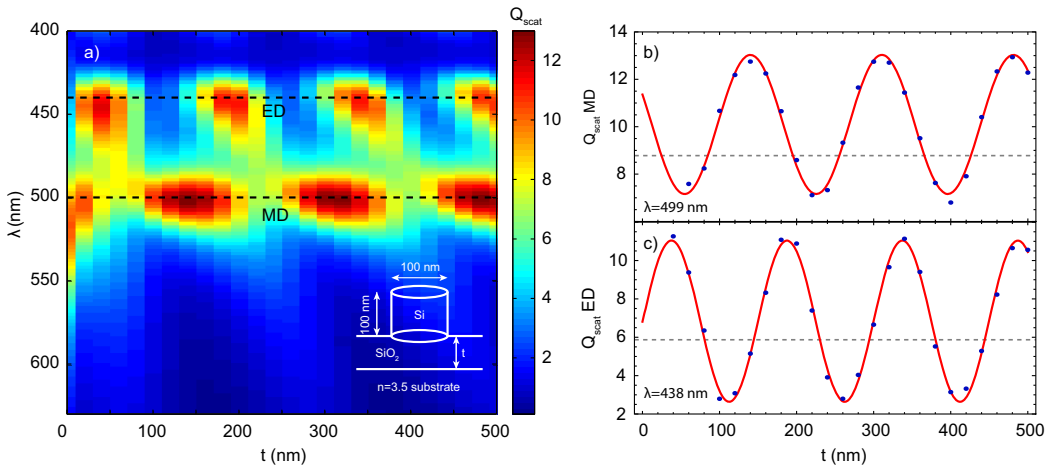

Fig. 5. **(a)** Q_{scat} as a function of wavelength and oxide thickness t, for a $d = 100$ nm, $h = 100$ nm Si cylinder, positioned on top of an oxide layer with thickness t, on top of a semi-infinite substrate with $n_{sub} = 3.5$. The inset shows the geometry. The horizontal black dashed lines indicate crosscuts at resonance wavelengths: $\lambda = 440$ nm (ED) and $\lambda = 499$ nm (MD). **(b-c)** Blue dots show the cross sections from (a), red lines show the fits from the interference model. The free-space wavelengths found from the fit are shown on the bottom left of the figures. The gray dashed lines show the peak value of Q_{scat} for the same particle on a semi-infinite SiO_2 substrate (limit of $t \to \infty$).

#195676 - $15.00 USD Received 27 Aug 2013; revised 11 Oct 2013; accepted 16 Oct 2013; published 25 Oct 2013

The results are shown in Fig. 5(a), where Q_{scat} is shown (color) as a function of t and λ. For $t = 0$, we observe one very broad peak: the resonator is strongly coupled to the substrate and the ED and MD mode broaden and overlap as in Fig. 4. However, as t increases Q_{scat} of the MD mode and ED mode are subsequently suppressed and enhanced. The horizontal dashed black lines indicate crosscuts near the resonance wavelength for the MD mode ($\lambda = 499$ nm) and the ED mode ($\lambda = 440$ nm), which are shown as blue dots in Figs. 5(b) and 5(c) respectively. Note that the oscillation period is different for the ED and MD modes as they appear at different wavelengths, such that any combination of MD/ED amplitude within the oscillation can be chosen: at $t \sim 400$ nm both modes are in phase while at $t \sim 60$ nm they are out of phase. This effect is caused by constructive and destructive interference of the incident light reflected from the SiO_2 layer, resulting in strong variations in the driving field in the resonator, as follows from a simple interference model. Indeed, the oscillation periods found in Figs. 5(b) and 5(c) correspond to the half-wavelength of light in the oxide layer.

To prove that this effect allows for both suppression and enhancement of one of the modes, the gray dashed lines in (b) and (c) show the peak value of Q_{scat} of the same particle on a semi-infinite substrate ($t \to \infty$) with index $n_{sub} = 1.5$ (roughly equal to n_{SiO_2}), which is 8.8 for the MD mode and 5.9 for the ED mode. As can be seen from both (b) and (c), the amplitude of Q_{scat} can both be lower and higher than these values. The modes are not fully suppressed since the amplitudes of the incoming light and the light scattered from the Fabry-Pérot cavity do not completely cancel each other.

7. Plane wave versus dipole excitation

All the above describes the resonant behavior of cylinders, illuminated by plane-waves under normal incidence. However, in many practical applications or experiments the driving field may be light under large angles of incidence (e.g. illumination through a large *NA* objective [11, 16]), or even a local source like an electron beam excitation [28], which corresponds to a vertically oriented electric dipole [29, 30]. Therefore, we investigate the resonant behavior of cylinders excited by a point dipole. We study the scattering cross section of a $d = 100$ nm, $h = 100$ nm Si cylinder in air and compare the data with those for plane wave illumination from the top (like in sections 3-6). Efficient driving occurs when the fields of the electric dipole source overlap those of the eigenmode. Thus, when the dipole is positioned in an anti-node if the eigenmode field profile. Here, we average over all dipole positions to find all eigenmodes that are efficiently excited by a vertical dipole. Note that this experimental configuration corresponds to that of cathodoluminescence spectroscopy, as we have recently shown for dielectric cylinders [28]. To simulate this, a vertically oriented electric dipole is positioned in the center of the particle, and then scanned to the edge of the particle in steps of 5 nm. For each step, a simulation is performed and the light scattered from the particle is collected using transmission monitors. Next, because of cylindrical symmetry, the dataset is rotated around the axis, and the total particle spectrum is obtained by adding all the individual spectra (using the proper Jacobian). Since the dipole driving power and plane wave base amplitude can be arbitrarily chosen, the spectra from both simulations are normalized for comparison. The results are shown in Fig. 6(a), where the blue line corresponds to dipole excitation and the red line to plane wave excitation. Both spectra show two peaks, corresponding to the MD mode at long wavelengths and the ED mode at short wavelengths. Interestingly, the figure indicates that both excitation mechanisms induce a similar MD mode, at the same wavelength, whereas the ED energies are distinctively different.

#195676 - $15.00 USD Received 27 Aug 2013; revised 11 Oct 2013; accepted 16 Oct 2013; published 25 Oct 2013

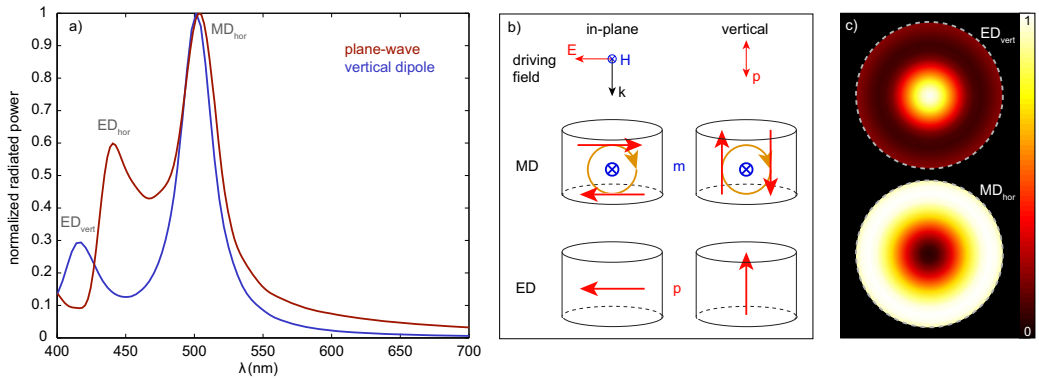

Fig. 6. **(a)** Normalized Q_{scat} for a Si cylinder with $d = 100$ nm, $h = 100$ nm in air under plane wave excitation (red), and excited by a vertically oriented electric dipole, calculated by integrating spectra obtained from scanning the dipole position over a horizontal cross-cut through the middle of the particle (blue). The modes are labeled in gray. **(b)** Excitation mechanism for the in-plane polarized plane wave source (left column) and vertically oriented electric dipole source (right column). The driving mechanism is shown for both the MD mode (top row) and ED mode (bottom row). The driving field orientation is shown on top. The orange circles indicate the displacement current loop inducing $\vec{m}$, the red arrows the E-field of the driving field (top row) and $\vec{p}$ orientation (bottom row). The blue crosses indicate the out-of-plane orientation of $\vec{m}$. **(c)** Excitation efficiency maps of the ED_{vert} (top) and MD_{hor} (bottom) modes driven by a vertically oriented electric dipole. The cross sections are taken at the particle half-height.

To further characterize this difference, we show in Fig. 6(b) the driving mechanisms of both the MD mode (top row) and the ED mode (bottom row), for the in-plane excitation using a plane wave (left column) and vertical dipole (right column). The driving field orientations are shown on top. For the plane wave driving field (left column), the excitation of the in-plane MD (labeled MD_{hor}) is a result of the E-field of light (red) coupling to a vertically oriented displacement current loop (orange), as was discussed in section 2. The projection of the driving field on the current loop determines the driving efficiency, which occurs on the top and bottom of the current loop in this case. Coupling of the plane wave to the in-plane ED (labeled ED_{hor}) mode (bottom left) occurs due to the in-plane polarization of the material by the driving field. The vertically oriented dipole excitation (right column) has the E-component of the driving field in the vertical direction. However, this driving field has good field overlap with the sides of the vertical displacement current loop, on the left and right of the particle (see top right in Fig. 6(a)). Therefore, the same *in-plane* $\vec{m}$ (MD_{hor}) can be induced with both vertical and in-plane E-fields, which explains why the peaks occur at the same resonance wavelength ($\lambda = 503$ nm).

The ED mode, however, is excited differently for the two cases. The ED mode excited by the vertical dipole source is vertically oriented (ED_{vert}), instead of horizontally. The different alignment of the dipole moment $\vec{p}$ within the particle causes the eigenmode to occur at different wavelengths: ED_{vert} (417 nm) occurs at shorter wavelengths than ED_{hor} (440 nm), as can be seen in (a). Note that if a horizontal point dipole would be coupled to the particle, the ED_{hor} mode occur at the same resonance wavelength, while the MD mode will change. Under these conditions, an in-plane current loop will be excited rather than a vertical one. So, the peak corresponding to MD_{hor} mode would occur in the spectrum, with a different resonance energy.

#195676 - $15.00 USD Received 27 Aug 2013; revised 11 Oct 2013; accepted 16 Oct 2013; published 25 Oct 2013

To further corroborate the excitation mechanisms by the vertical point dipole, Fig. 6(c) shows the excitation efficiency maps (corresponding to horizontal crosscuts of the mode profiles at the particle half-height) for the ED_{vert} (top) and MD_{hor} mode (bottom). These maps show how much light is scattered by the particle at resonance wavelength (20 nm bandwidth) as a function of the excitation position (position of the dipole). This corresponds to the coupling efficiency, which is determined by the field overlap of the eigenmodes and the E-fields of the dipole. Figure 6(c) shows that the ED_{vert} (top) is excited most efficiently when the dipole is positioned in the center (bright spot), which corresponds to the position of the vertically oriented $\vec{p}$ (see bottom right in (a)). Note that the slightly brighter ring on the outside is caused by inefficient coupling to the vertical component of the field lines of the ED_{hor} mode [31]. The MD_{hor} mode is excited most efficiently when the dipole is positioned in the bright ring on the edge of the particle, in agreement with the top right sketch in (a). Note that a ring is observed because the MD_{hor} mode is infinitely degenerate with respect to ϕ, which is a result of the cylindrical symmetry of the particle.

8. Radiation patterns

One of the most important characteristics of dielectric resonators is the angular radiation pattern. As specific eigenmodes are often characterized by distinct radiation profiles [28], this allows for the design of angular or spectrally sensitive photodetectors, and solar cell geometries with optimized light trapping. For resonators that are strongly coupled to a high-index substrate, a large fraction of the scattered light is emitted into the substrate due to the enhanced *LDOS* [32]. Here, we use the far-field transformation routine of Lumerical [25] to calculate the radiation patterns of single silicon scatterers on a substrate under plane wave illumination. We use a large (2.2 μm × 2.2 μm × 0.8 μm) simulation volume and apply the far-field transformation to the light propagating downward into a semi-infinite substrate with index n_{sub}, collected by a monitor outside the TFSF source (150 nm below the air-substrate interface). In this way, the radiation patterns only include the scattered light and not the incident light.

Figure 7(a) shows Q_{scat} of a Si cylinder with $d = 100$ nm, $h = 100$ nm on a semi-infinite substrate with $n_{sub} = 1.5$ (red) and $n_{sub} = 3.5$ (blue). The geometry is shown as an inset, where we define θ as the angle with respect to the surface normal pointing downward. For $n_{sub} = 1.5$, we observe two distinct resonances due to the ED mode (labeled 1) and the MD mode (2). For $n_{sub} = 3.5$, both peaks have broadened such that they spectrally overlap and the resonant response is dominated by the MD mode (3).

Figure 7(b) shows the fraction of the scattered power that is scattered into the substrate as a function of n_{sub}, integrated over all wavelengths (red) and at the MD resonance wavelength (blue). Both lines show an increase in downward scattering with increasing n_{sub} due to the increased *LDOS* [32]. For $n_{sub} = 3.5$ (close to n_{Si}) more than 80% of the scattered light goes into the substrate. Indeed, arrays of Si nanocylinders have shown to act as efficient anti-reflection coatings [23]. Surprisingly, this scattering fraction is lower at resonance than it is for the total power, which shows that the directionality is not optimum at the resonances wavelength itself. However, the absolute power scattered into the substrate *is* determined by Q_{scat} and does peak at resonance (also see Fig. 8).

To show that the individual resonances can be used as directional antennas, we show in Fig. 7(c) the angular radiation profiles into the substrate for the Si cylinder (top row), as a function

#195676 - $15.00 USD Received 27 Aug 2013; revised 11 Oct 2013; accepted 16 Oct 2013; published 25 Oct 2013

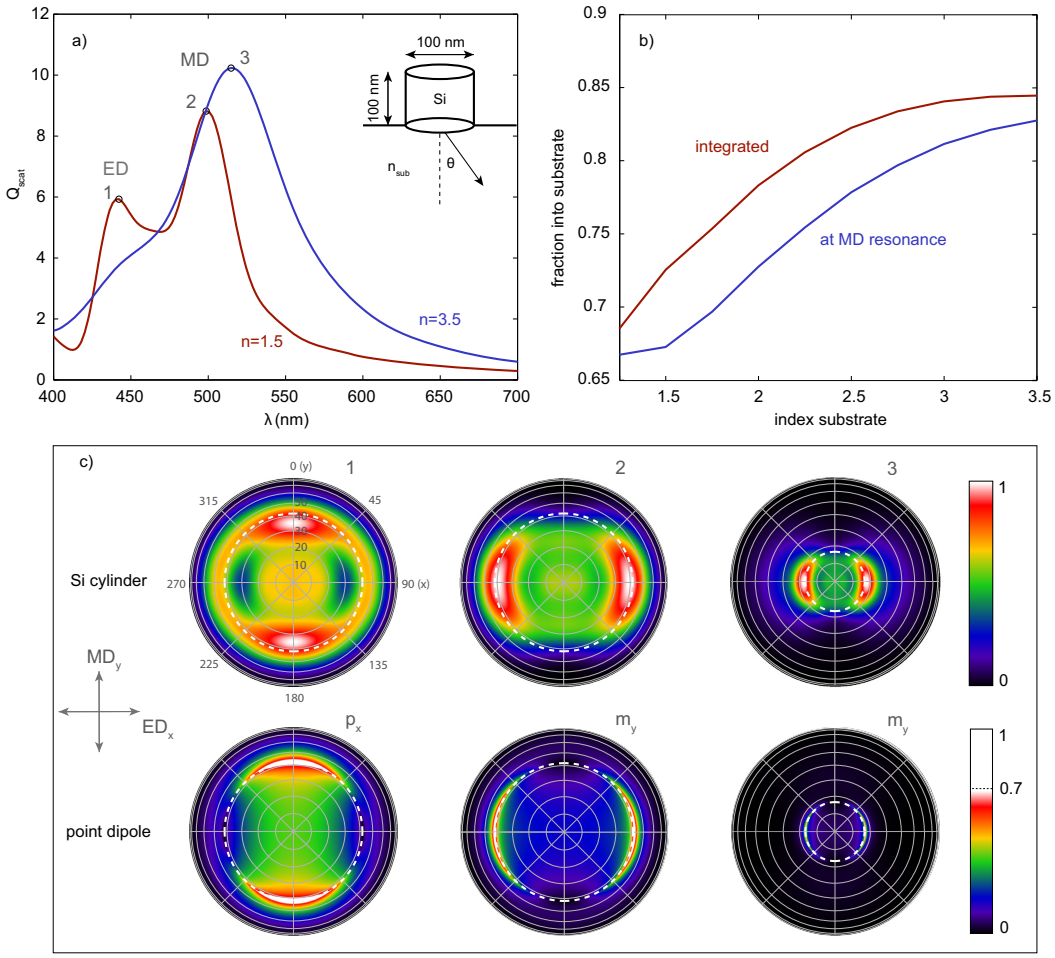

Fig. 7. **(a)** Q_{scat} for a Si cylinder with $d = 100$ nm, $h = 100$ nm positioned on a semi-infinite substrate with $n_{sub} = 1.5$ (red) and $n_{sub} = 3.5$ (blue). The geometry is shown as an inset. The peaks are labeled according to the corresponding resonance (ED / MD) and numbered for reference in (c). **(b)** fraction of scattered power into the substrate as a function of n_{sub}, at resonance wavelength (blue) and integrated over the entire spectral range ($400 - 700$ nm). A clear increase in downward scattered power is observed with increasing n_{sub}, attributed to the enhanced *LDOS* in the substrate. **(c)** Far-field radiation patterns for the numbered peaks from (a) corresponding to the ED and MD modes of the Si cylinder (top row). $1 - 2$ correspond to the ED and MD mode on a $n_{sub} = 1.5$ respectively, 3 to the MD mode on $n_{sub} = 3.5$. The gray circles correspond to constant θ with equidistant spacing $\Delta\theta = 10^{\circ}$. The white dashed circles correspond to the critical angle θ_c in the substrate. The orientation of the ED and MD dipole moments are shown on the left. The bottom row shows the calculated radiation patterns of the corresponding point-dipoles (p_x and m_y), positioned 50 nm above the substrates with $n_{sub} = 1.5$ (left, center) and $n_{sub} = 3.5$ (right). Note that the colorbar of the bottom row has been saturated at 0.7 for visibility.

of azimuthal angle and zenithal angle. From left to right, the patterns correspond to peaks $1 - 3$ in Fig. 7(a), respectively. Incident light is polarized along $\hat{x}$, i.e. the $\theta = 90^{\circ}$ direction. The orientation of the ED and MD dipole moments is shown by the gray arrows on the left.

#195676 - $15.00 USD Received 27 Aug 2013; revised 11 Oct 2013; accepted 16 Oct 2013; published 25 Oct 2013

Furthermore, the critical angle for light trapping in guided modes is plotted as a white dashed line in each radiation pattern.

Radiation pattern 1 shows clear beaming from the ED mode into two specific angular lobes along $\hat{y}$, close to the critical angle. The radiation pattern of the MD mode (pattern 2) shows similar directional beaming close to the critical angle, but now along $\hat{x}$. The orientation of the radiation patterns correspond to that of an electric dipole and magnetic dipole on a substrate, oriented in the $\hat{x}$-direction (p_x) and $\hat{y}$-direction (m_y) respectively. To show this, we also plot the radiation profiles into the substrate of point dipoles (p_x, bottom left, and m_y, bottom center and bottom right) positioned 50 nm above a substrate with $n_{sub} = 1.5$ (bottom left and bottom center) and $n_{sub} = 3.5$ (bottom right). The radiation patterns are obtained from classical theory [33, 34]. Comparing radiation patterns 1 and 2 with those of p_x and m_y we find qualitative agreement, indicating that 100 nm high cylindrical particles at resonance have radiation patterns similar to point dipoles. Finally, radiation pattern 3 in Fig. 7(c) shows how the radiation pattern of the $\hat{y}$-oriented MD (MD_y) resonance is influenced by an increase in refractive index of the substrate to $n_{sub} = 3.5$. The same directional beaming is observed, but now more pronounced (stronger beaming) and under smaller θ as the critical angle has decreased to $\theta_c = 16.6^\circ$. Again, good qualitative agreement is observed with the point dipole model (bottom right).

The patterns observed in Fig. 7(c) show that selective excitation of eigenmodes (ED or MD) allows for directional emission in the $\hat{x}$ or $\hat{y}$-direction. Therefore, the combination of spectrally separated ED/MD modes can be used for wavelength demultiplexing of polarized light: short wavelengths are scattered along $\hat{y}$ by the ED mode, long wavelengths along $\hat{x}$ by the MD mode. The height and diameter can be tuned to obtain the desired spectral response, the index of the substrate defines the bandwidth and scattering angle (i.e. SiO_2 gives large angles). Furthermore, the strong emission around the critical angle has direct implications for the use of such resonators for light trapping in weakly absorbing substrates, such as solar cells. Note that Fig. 7 only considers the radiation patterns of the lowest order dipolar modes. It has been observed that higher order modes show strong beaming around the normal [28]. Furthermore, the patterns observed in Fig. 7(c) change when the particle gets taller. In this case, the effective dipole moments are positioned further away from the substrate, such that a larger fraction of the emission is below the critical angle. Simulations show that increasing the particle height from 100 nm to 200 nm significantly changes the radiation patterns from dipolar like emission profiles as observed in Fig. 7(c), to strong beaming along the normal due to the increased distance of the effective dipole moments to the substrate. Altogether, this indicates that tuning the geometry of the resonator can give accurate control over the radiation properties of the scattered light.

Figure 8(a) shows a comparison of the forward (green) and backward (blue) scattered power for a $d = 100$ nm, $h = 100$ nm Si cylinder on a substrate with $n_{sub} = 1.5$. Also shown are the ratio P_{down}/P_{up} (red), and the spectral range of the ED (shaded red) and MD (shaded blue) resonances. Note that the oscillations in the red line for $\lambda > 580$ nm are due to numerical noise. The scattering ratio peaks at 14.8, which indicates strong directional scattering into the substrate. This is a result of the interference of light scattered by the ED and MD modes, as was theoretically predicted by Kerker et al. [35] and recently demonstrated experimentally for spheres [11, 20] and cylinders [21]. For Si spheres, the peak ratio observed was ~ 8 [11], which shows that particles that have strong coupling to a substrate can exceed this ratio significantly.

#195676 - $15.00 USD Received 27 Aug 2013; revised 11 Oct 2013; accepted 16 Oct 2013; published 25 Oct 2013

However, in the latter case the directionality also originates from the high *LDOS* of the substrate. To differentiate these two effects, Fig. 8(b) shows the ratio P_{down}/P_{up} as a function of wavelength for $1.25 \leq n_{sub} \leq 3.5$ in steps of 0.25. As was observed in Fig. 4(a), with increasing n_{sub} both the ED and MD resonance peaks significantly broaden and the total scattered power increases. The peak scattering ratio is significantly reduced for larger n_{sub}. Thus, the contrast from the ED/MD interference is strongly suppressed, whereas the average value is similar (6.4 for $n_{sub} = 3.5$, 6.8 for $n_{sub} = 1.5$). Therefore, this graph clearly shows the trend from scattering dominated by Kerker-type interference (high peaks and dips, low n_{sub}) to scattering dominated by *LDOS* (flat and high response, for high n_{sub}). The reason for this transition can be understood from the requirements for Kerker-type interference: as n_{sub} increases, the overlap in the far-field radiation patterns is reduced and the relative phase difference is less well defined. The combination of Kerker-type interference and *LDOS* dominated scattering can be tuned to get optimum directionality for one specific wavelength, or reduced directionality over a broad spectral range. Note that the optimum in forward scattered power always occurs at the MD resonance (see also Fig. 7(b)) [21].

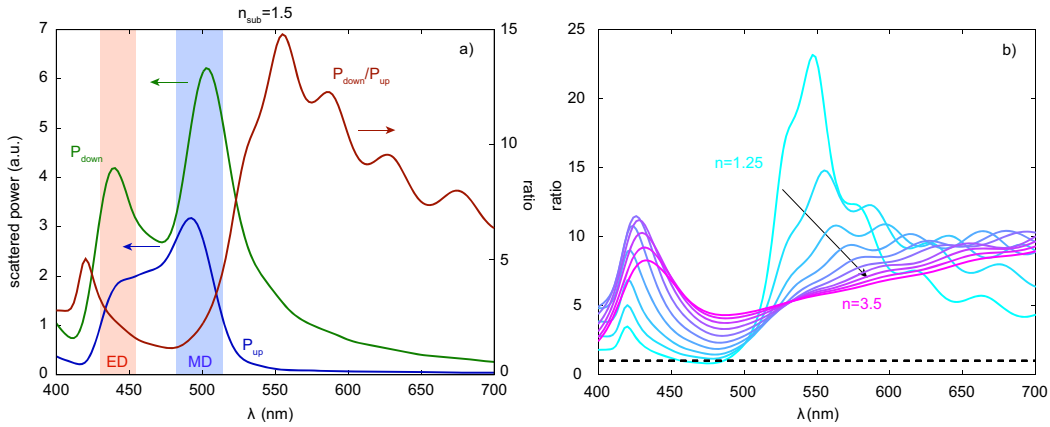

Fig. 8. **(a)** Back scattered power (blue), forward scattered power (green) and forward/backward ratio (red) for a $d = 100$ nm, $h = 100$ nm Si cylinder on $n_{sub} = 1.5$. The red and blue shaded regions indicate the spectral reange of the ED and MD resonances respectively. Note that the oscillations in the red curve for $\lambda > 580$ nm are due to numerical noise. **(b)** Forward/backward scattering ratio as a function of wavelength for different n_{sub} ranging from 1.25 to 3.5 in steps of 0.25.

9. Conclusions

In conclusion, we have systematically studied the influence of particle geometry and dielectric environment on the resonant behavior of single dielectric particles, both isolated and strongly coupled to a substrate. We found that the lowest energy mode is an in-plane MD mode, driven by a vertical displacement current loop inside the particle. In the limit of low n and low h, there is not enough retardation to form a current loop, such that no MD mode is supported. The excitation of the ED mode is not limited by such constraints. At larger diameters, the ED and MD spectrally overlap, and the higher order MQ mode appears in the blue spectral range. Furthermore, we observe that strong coupling to (dielectric) substrates requires a large contact area between the resonator and the substrate. This allows the displacement current loop to extend partially into substrate, yielding high radiative losses into the substrate. More complex multi-layer substrate allow selective enhancement and/or suppression of ED and MD modes

#195676 - $15.00 USD Received 27 Aug 2013; revised 11 Oct 2013; accepted 16 Oct 2013; published 25 Oct 2013

through coupling with a Fabry-Pérot mode in the multi-layer substrate. Also, by comparing dipole and plane wave sources, we found that both vertical and horizontal E-fields can excite the in-plane MD mode, whereas the ED modes have orthogonal dipole moments and different resonance energies. Finally, by studying radiation patterns into the substrate we found that the ED and MD modes have radiation patterns similar to point dipoles above substrate, showing strong directional beaming around the critical angle. Altogether, this work is a guideline for the engineering of dielectric resonators, which allows one to use the combined scattering from ED and MD modes to taylor the scattering properties for specific applications.

Acknowledgments

We would like to thank Toon Coenen for useful discussions and careful reading of the manuscript. Furthermore, we acknowledge Femius Koenderink for providing the magneto-electric point-dipole code for calculating far-field radiation patterns. We thank SARA Computing and Networking Services (www.sara.nl) for their support in using the Lisa Compute Cluster. This work is part of the research program of the Stichting voor Fundamenteel Onderzoek der Materie (FOM), which is financially supported by the Nederlandse Organisatie voor Wetenschappelijk Onderzoek (NWO). This work was also funded by an ERC Advanced Investigator Grant.

#195676 - $15.00 USD Received 27 Aug 2013; revised 11 Oct 2013; accepted 16 Oct 2013; published 25 Oct 2013